WELDING RESEARCH

SUPPLEMENT TO THE *WELDING JOURNAL*, JUNE 2000
Sponsored by the American Welding Society and the Welding Research Council

Stress Relaxation Study of HAZ Reheat Cracking in Type 347 Stainless Steel

Gleeble™-based stress relaxation tests evaluate a material's susceptibility to weld HAZ reheat cracking

BY L. LI AND R. W. MESSLER, JR.

ABSTRACT. Four different compositions of Type 347 austenitic stainless steel were studied using Gleeble™-based stress relaxation tests to evaluate susceptibility to weld HAZ reheat cracking. Coupons extracted from plate were thermally cycled to reproduce the coarse-grained region of the HAZ known to be most prone to such cracking. These samples were then reheated to various PWHT temperatures, and a strain comparable to 70% of the strain to cause yielding at the temperature was applied. Force in the specimens was recorded for up to 3 h while this total strain was kept constant. Force vs. time curves for all samples exhibited an increase attributed to volumetric shrinkage upon precipitation of Nb-rich particles as confirmed by constant-stress tests. Formation of Nb-rich precipitates strengthens the alloy, and stress buildup due to volumetric shrinkage in the age-hardening matrix leads to cracking along grain boundaries when stress cannot relax fast enough by yielding or creep.

Introduction

Type 347 stainless steel, as well as other Nb-containing Fe- and Ni-based austenitic alloy weldments, have been and continue to be plagued by cracking. Such cracking occurs frequently in the weld fusion zone (FZ) and/or the heat-affected zone (HAZ) during welding, occasionally in the HAZ during postweld heat treatment (PWHT) and, as found more and more with increasing experience, in HAZs following extended service at elevated temperatures (Ref. 1). This article reports the results of a study on the role of base metal composition and microstructure on HAZ reheat cracking.

Factors affecting reheat or strain-age cracking susceptibility during PWHT of ferrous and nonferrous alloys exhibiting precipitation of strengthening second-phase particles have been identified as 1) development of coarse grain size and dissolution of second-phase particles in the HAZ during welding, 2) reheating that causes re-precipitation of fine particles within grains and grain boundaries to cause hardening and loss of ductility, and 3) joint geometry and thermal history that determine the amount and rate of stress relaxation during reheating (Ref. 2). Postweld stress-relief cracking is generally limited to thick-walled vessels made from higher-alloy, high-temperature, creep-resistant grades such as austenitic stainless and Cr-Mo-V steels (Ref. 3). Cracking occurs early in the reheat cycle and can be located in the coarse-grained weld metal, but is more commonly located in the less strain-tolerant, coarse-grained region of the HAZ (Ref. 4). It has been postulated that NbC and Nb(C,N) precipitates strengthen the matrix to the extent that most of the relaxation of stress takes place along grain boundaries (Refs. 3, 5). When the strain from welding or heat treatment or service-induced thermal cycles exceeds a critical value, intergranular cracking occurs.

KEY WORDS

Austenitic Stainless Steel
Type 347
Reheat Cracking
Stress Relaxation
Gleeble™

Stress relaxation as a means for studying reheat cracking in austenitic alloys has been employed by numerous researchers (Refs. 6–10). In an as-welded joint, there are multi-axial stresses and elastic strains. No change in the physical size of the weld joint occurs as weld-induced stresses are relieved by postweld thermal cycles, at least for heavy-section weldments. Thus, the total strain in the weld joint remains constant. This condition of constant total strain is the principal factor that must be present in any test to study cracking during postweld heat treatment (Ref. 6).

L. LI is a doctoral candidate and R. W. MESSLER, JR., is Professor in Materials Science and Engineering at Rensselaer Polytechnic Institute, Troy, N.Y.

Based on a paper presented at the 79th Annual AWS Convention in Detroit, Mich., April 26–30, 1998.

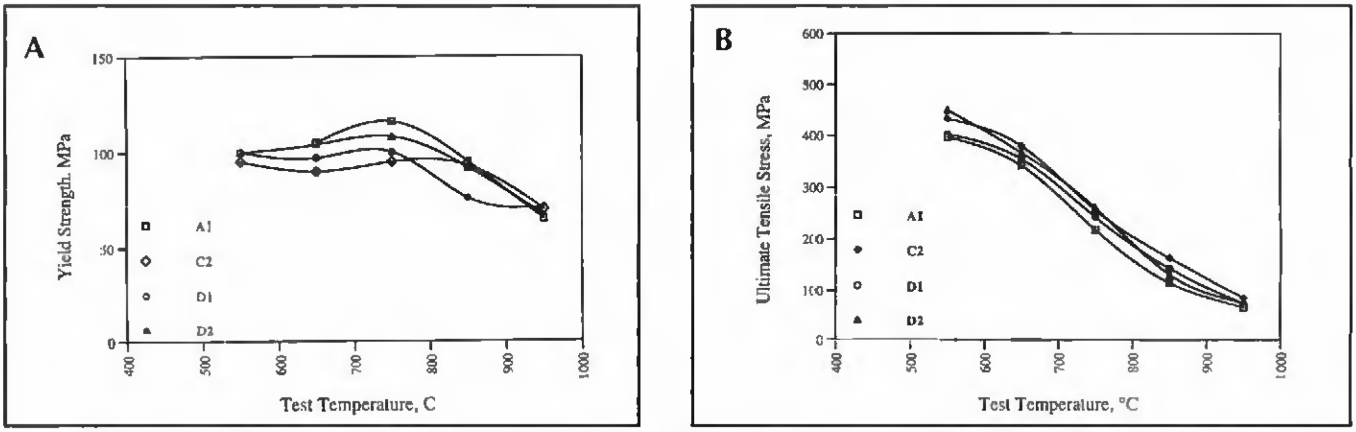

Fig. 1 — Yield strength (A) and ultimate tensile strength (B) of test Type 347 at different temperatures.

In a stress relaxation test, total strain (ε_T) remains constant. Plastic strain (ε_p) accumulates at the expense of elastic strain (ε_e), so the relation $\varepsilon_T = \varepsilon_e + \varepsilon_p$ holds true for the test. Stress relaxation is a straightforward and sensitive method for providing a guide to metallurgical events such as recrystallization and precipitation (Ref. 11). During a stress relaxation test, stress or force vs. hold time can provide information on susceptibility to reheat cracking during postweld heat treatment or other thermal exposure.

Experimental Procedure

Samples of commercially available Type 347 stainless steel plates with four different compositions within the specification for standard or nuclear grades (Table 1) were tested and compared. The experimental procedure involved the following: 1) Instron-based hot tensile tests of base materials, 2) Gleeble weld thermal cycle simulation to develop susceptible HAZ microstructure, 3) notching of test specimens to facilitate cracking, 4) Gleeble-based stress relaxation tests, 5) data analysis, 6) metallographic observations and 7) correlation of test results and microstructure.

Hot tensile tests were conducted on as-received materials to determine appropriate initial stresses and strains for stress relaxation tests. Tensile stress-strain behavior was measured with smooth samples for temperatures between 550 and 950°C. All tensile tests were performed using an Instron Model 8562 Electro-Mechanical Testing System with self-aligning grips and a computer-based data acquisition system, along with a split, resistance-heated furnace. The samples were uniformly heated at 50°C/min from room temperature to test temperatures, and loading was started 1 min after arriving at the test temperature. The strain rate for tests was 0.04/min. Results obtained are plotted in Fig. 1 as yield and tensile strength vs. test temperature.

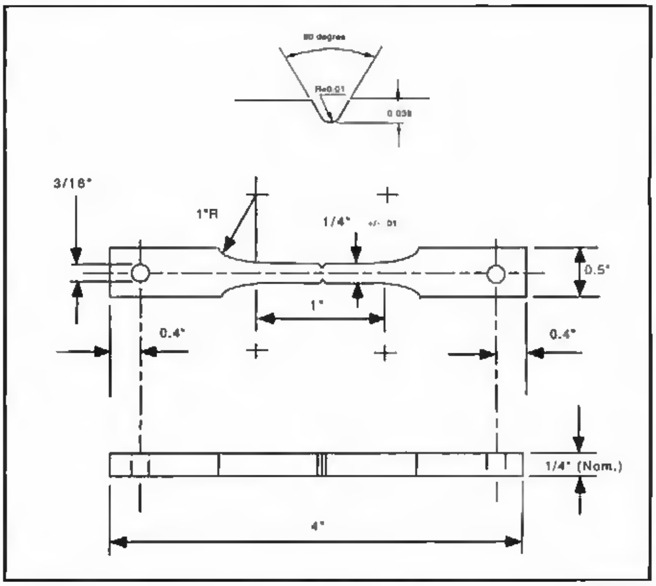

Fig. 2 — Sample geometry for the Gleeble stress relaxation tests.

An upgraded Model 1500 Gleeble™ (produced by DSI, Poestenkill, N.Y.) was used to simulate key weld thermal cycles in coupons with a 6.4 x 6.4-mm square section. A 1300°C peak temperature with 1.1 kJ/mm (28 kJ/in.) heat input was employed in the Gleeble simulations to produce the structure found in the coarse-grained HAZ (CGHAZ) of welds, where

Table 1 — Four Different Compositions of Type 347 Stainless Steel

Code	C	Si	Mn	P	S	Cr	Ni	Mo	N	Nb	Co	Cu	Al	Ti	Sn	Nb/C	PN measured
A1 (347NG)	0.022	0.32	1.51	0.025	0.004	17.68	10.48	0.24	0.036	0.4	N/A	N/A	N/A	N/A	N/A	18.2	1.3
C2 (T347)	0.05	0.59	1.57	0.025	0.025	17.75	9.53	0.33	0.032	0.59	0.09	0.23	N/A	0.003	N/A	11.8	1.6
D1 (T347)	0.023	0.48	1.66	0.031	0.007	17.74	10.27	0.35	0.021	0.367	0.1	0.32	0.001	0.005	0.022	16	3.2
D2 (T347)	0.044	0.57	1.42	0.03	0.001	18.2	10.63	0.27	0.044	0.48	0.19	0.33	0.001	0.007	0.018	10.9	0.7

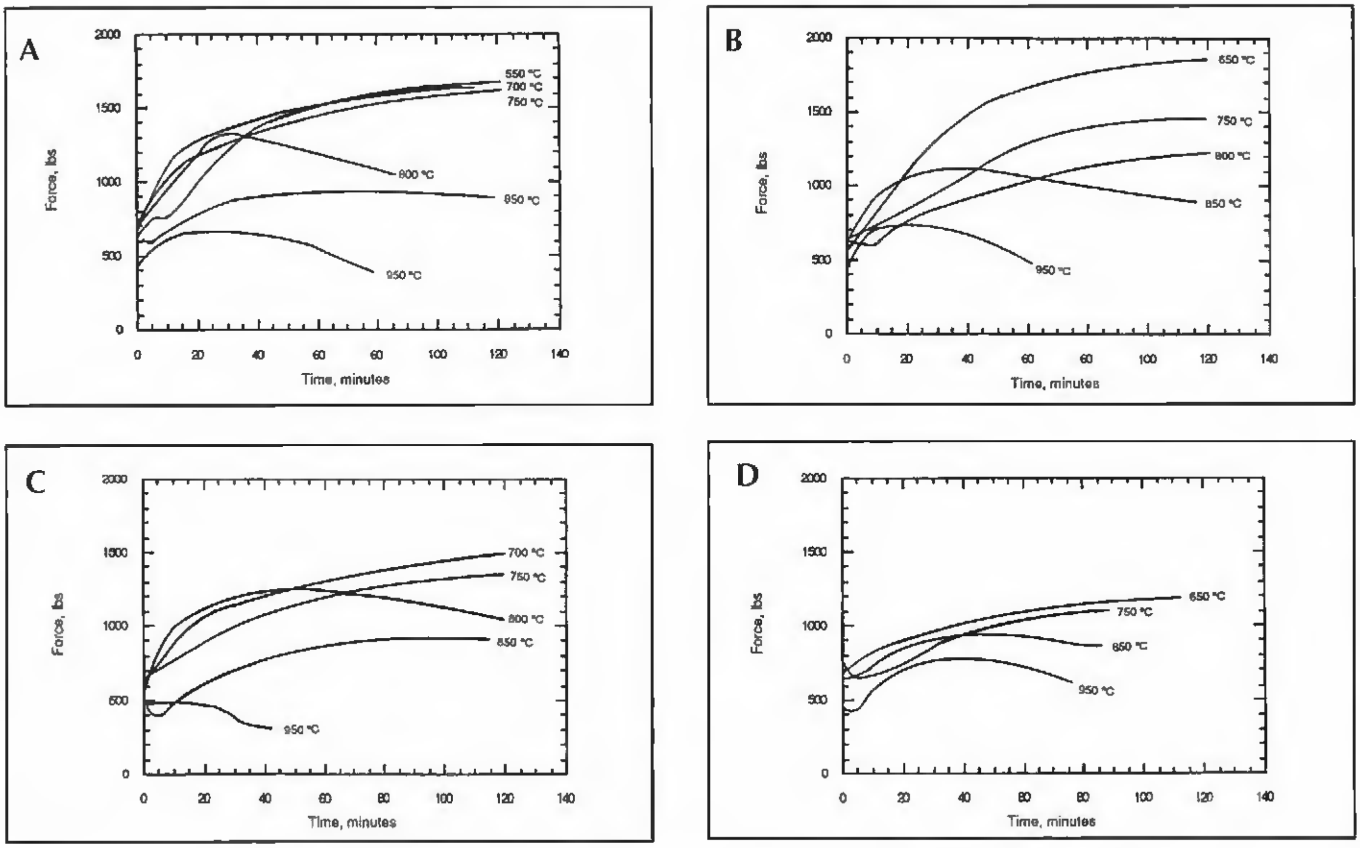

Fig. 3 — Force vs. time curves from the stress relaxation tests: A — A1; B — C2; C — D1; D — D2.

tolerance to strain from any source (external or internal) is known to be lowest (Ref. 4).

Gleeble-based stress relaxation tests were performed by bringing the square-section samples to test temperatures in the range of 550 to 950°C at a heating rate of 50°C/min, then applying a strain (via the Gleeble's stroke control) to 70% of the strain at yield at the test temperature. The selection of 70% yield-strain level was somewhat arbitrary because, qualitatively, any initial residual stress level (assumed to be at the yield stress) in actual welds would decrease during the heating process (Refs. 6, 10). However, 70% yield-stress (equivalent to 70% strain within the elastic region) is widely used as a design allowable for yield-limited designs (Ref. 12). Once the strain level was adjusted to the predetermined value, sample extension was kept constant throughout testing while force was recorded vs. time over a period typically of 3 h. The 3-h time period was employed because of the convenience of testing and because long stress-relief cycles are economically burdensome. The resulting force-time curves were analyzed, and tested samples were metallographically examined for cracks.

Preliminary tests with Type 347 showed smooth bars did not produce cracks during relaxation. Previous work by others also confirmed stress concentration as one of the conditions exacerbating reheat cracking (Ref. 8). In fact, smoothing the joint by grinding after welding was found effective for preventing reheat cracking in Type 347 (Ref. 9). Thus, all thermally cycled specimens were notched to give a nominal stress concentration factor of K = 3.3. The final geometry for stress relaxation specimens, including notch dimensions, is shown in Fig. 2. Note that notch dimensions are not the same as for a standard Charpy V-notch specimen.

Results and Discussion

Force vs. time curves, as shown in Fig. 3A–D, generally exhibited a small decrease during the initial relaxation stage, lasting 1 to 5 min, with force then gradually increasing. Force eventually decreases when relaxation time is extended sufficiently at any exposure temperature, with the time required being dependent upon the relaxation mechanism kinetics. Complete fracture of the sample seemed to be associated with force-time curves exhibiting a distinct peak (within the 3-h maximum test period). Crack initiation was always observed in those samples in which force-time curves exhibited such a peak (again, within the 3-h test period).

Specimen examination showed cracking at the root of notches after testing over a range of temperatures. The deepest cracks occurred in all test alloy compositions after exposure to relaxation temperatures that produced a peak in the force-time curve (again, within the study's 3-h period). The decrease in force was related to cracking that produced a decrease in cross section.

Figure 4A–D compares cracking among the tested alloys. Specimens with composition D2 exhibited complete fracture, indicating D2 is the most susceptible among the tested compositions to reheat cracking during PWHT. Lower temperatures than what produced a peak in the force-time curve (e.g., 750 vs. 800°C for D2), resulted in less severe cracking for all tested compositions. The highest temperature tests (>850°C) were characterized by a low peak load and a short failure time. Here, specimens necked during testing, and failure was by a stress-rupture mode characterized by dynamic recrystallization, wedge-type cracking and formation of cavities at grain boundaries — Fig. 5.

The as-received optical microstruc-

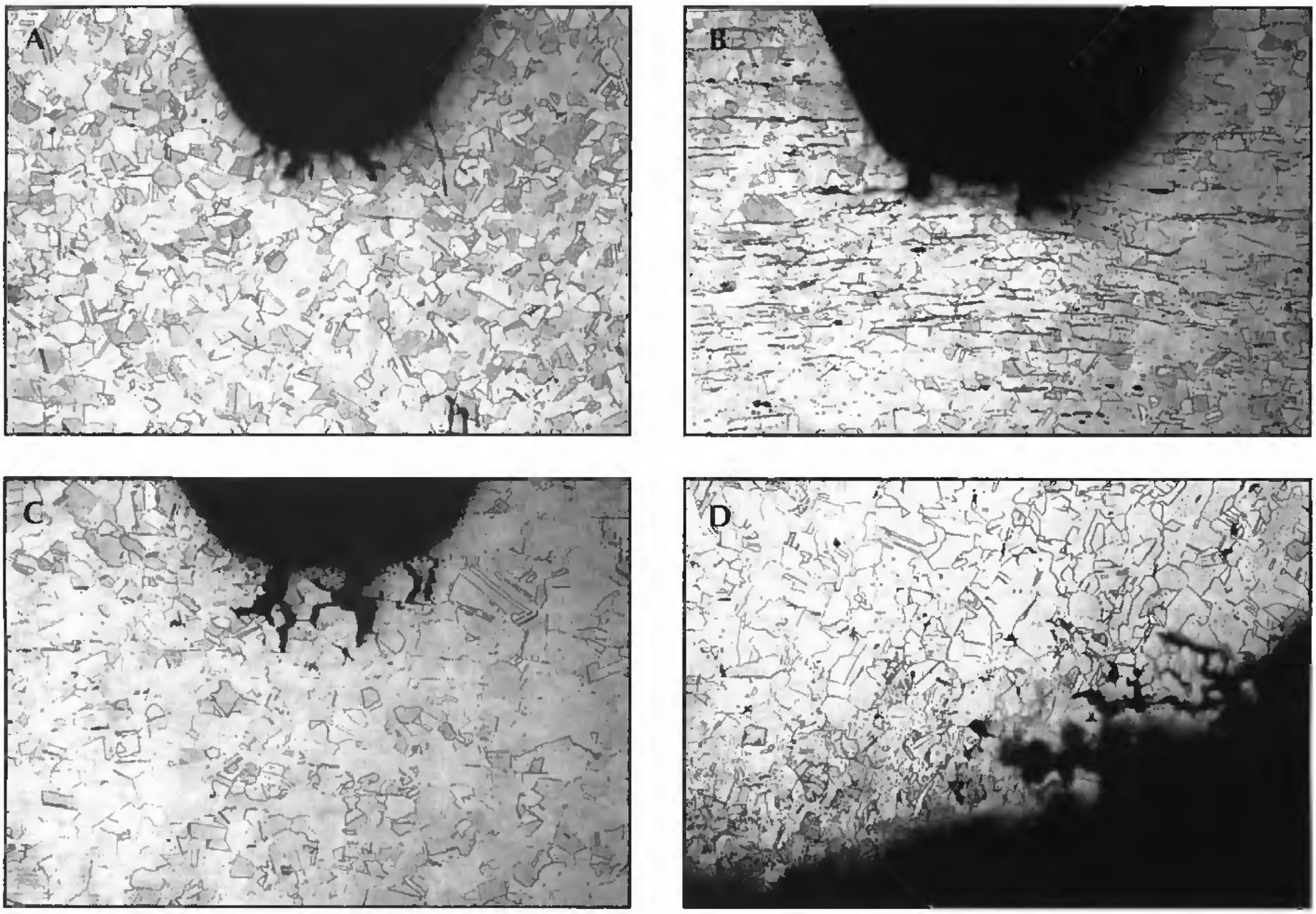

Fig. 4 — Cracking at root of notches (50X) after 3-h stress relaxation tests at temperatures that produced peaks in the force-time curves: A — A1 tested at 850°C; B — C2 at 850°C; C — D1 at 800°C; D — D2 at 800°C.

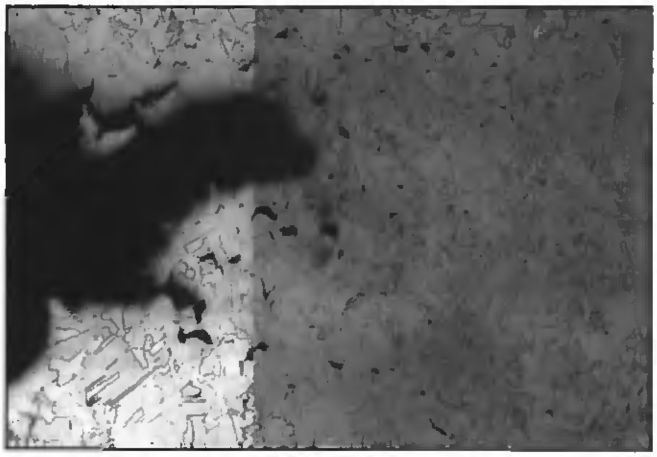

Fig. 5 — Cross-sectional view of the fractured region in D2 after a 3-h stress relaxation at 950°C (25X).

ture of test alloys shows an austenite matrix with some Nb-containing particles in the matrix. As an example, the microstructure of D2 before and after a 1300°C peak thermal cycle is shown in Fig. 6. Note in Fig. 6B the virtual absence of particles of Nb compounds at grain boundaries after the thermal cycle. This microstructure of as-cycled D2 before reheat testing was similar to the as-welded condition for the HAZ near the zero ductility temperature (ZDT). After a 550°C relaxation test, the microstructure was nearly the same as that of the as-cycled sample. The microstructure of D2 after a 700°C relaxation test showed sparse precipitates decorating grain boundaries — Fig. 7. Under higher-magnification SEM, smaller precipitates are abundantly distributed inside grains as well. The microstructure of D2 after a 750°C relaxation test showed more prevalent precipitates at grain boundaries, with some grain growth of the austenite matrix — Fig. 8. The microstructure of D2 after an 800°C relaxation test showed small, newly formed austenite grains and wedge-type grain boundary openings for force-time curves that peaked within the 3-h test. Some grain boundaries were free of the precipitates observed after lower temperature exposure, though the intragranular precipitates were readily seen optically — Fig. 9.

Precipitate-free grain boundaries were also observed in other alloy compositions tested — Figs. 10–12. Compared with the precipitate-strengthened matrix, precipitate-free grain boundaries may experience more deformation and crack initiation through grain boundary sliding (Ref. 13). Such grain boundary sliding is suggested by the presence of both w-type (at grain corners, Fig. 9) and r-type (at grain edges, Fig. 12) cavities in the tested samples. The definitions for w-type and r-type cavities and their being indicative to grain boundary sliding are discussed in Ref. 14.

The reason for a force increase during

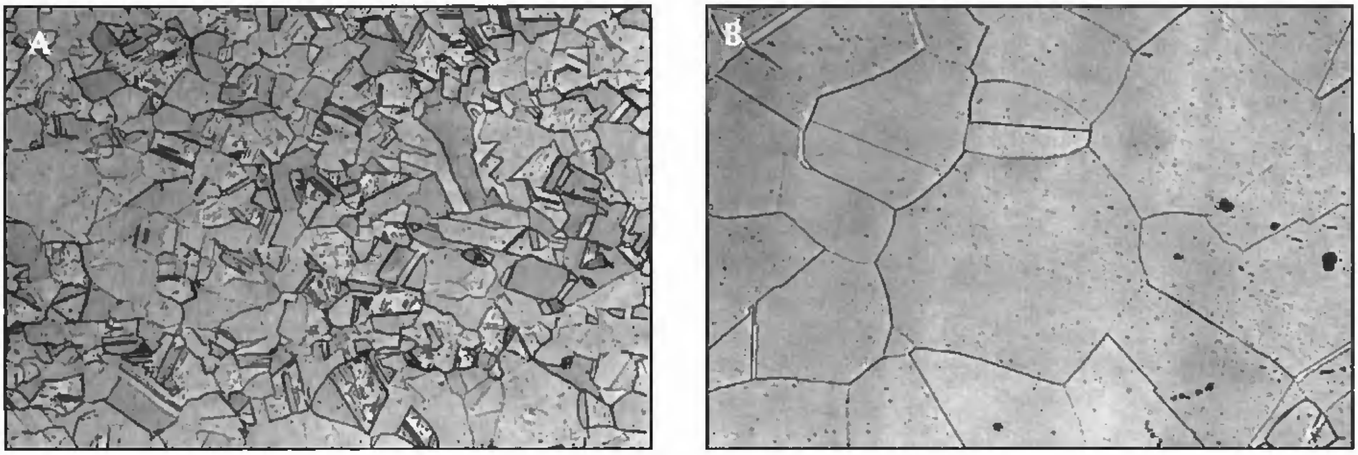

Fig. 6 — Microstructure of (A) as-received and (B) after 1300°C-peak thermal cycle for D2 composition (400X). Note virtual absence of particles of Nb compounds at grain boundaries.

Fig. 7 — Microstructure of D2 after 700°C relaxation test (400X) showing sparse, fine precipitates at grain boundaries.

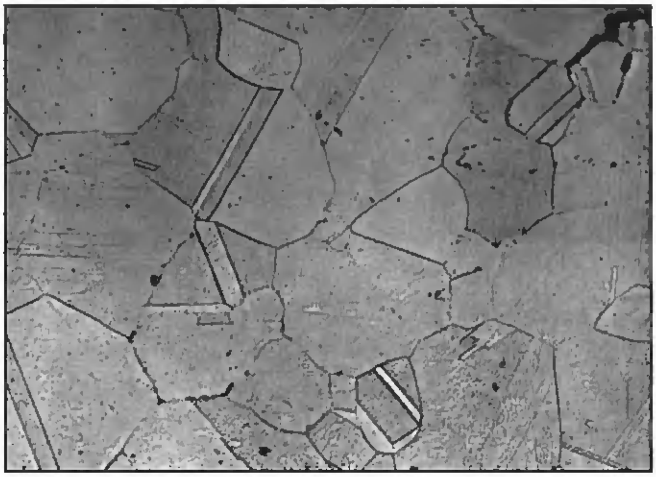

Fig. 8 — Microstructure of D2 after 750°C relaxation test (400X) showing larger, but still sparse, precipitates at some grain boundaries.

initial relaxation has been suggested to be due to shrinkage in a Gleeble stress relaxation study of a Ni-based alloy (Ref. 7). To confirm this shrinkage mechanism in Type 347, a constant stress test was employed. If the sample became shorter during constant-strain stress relaxation, then, for a constant-stress condition at the same temperature and stress level, the strain in the sample should exhibit a negative change, *i.e.*, volumetric shrinkage was occurring.

Verification tests were conducted on an Instron Model 8562 mechanical testing machine with a precise high-temperature extensometer and computer-controlled loading system. The gauge length of the test coupon was 25 mm. During tests, samples of the same notch geometry and microstructure as used in Gleeble stress relaxation tests were heated at 50°C/min to 750°C. When temperature equilibrated, stress of 70% yield strength (equivalent to 70% strain at yield) at 750°C was applied in 30 s and kept constant throughout a 3-h test, while strain was recorded.

A typical strain-vs.-time curve obtained from this constant-load test is shown in Fig. 13. The curve clearly shows a small (15%) but definite decrease of strain with time at the test temperature, indicating the specimen shortened during a hold at 750°C. From these confirming tests, shrinkage during reheating of Type 347 has been identified and the force-time behavior from relaxation tests can readily be understood. Incidentally, this dimensional change is different from dimensional changes that are solely temperature dependent and completely reversible arising from normal thermal expansion and contraction. The shrinkage under discussion is of metallurgical origin, involving phase or other structural changes, such as carbide precipitation.

The cause of confirmed shrinkage is believed to be a decrease in the specific volume of the alloy during the precipitation process. An EDS analysis (Fig. 14) of precipitates in relaxation-tested samples shows precipitates are Nb-rich phases, likely Nb-carbides and nitrides. Accompanying the precipitation, there are changes in specific volume of the solid solution matrix and contributions from concurrent appearance of carbide phases.

To understand the kinetics of stress relaxation and precipitation, the relaxation results are plotted as stress vs. logarithmic time. As in Fig. 15, all curves show an initial linear portion lasting up to 5 min with a slightly negative slope. This portion can be regressed to the following form:

$$\sigma = \sigma_0 - k\ln(t)$$

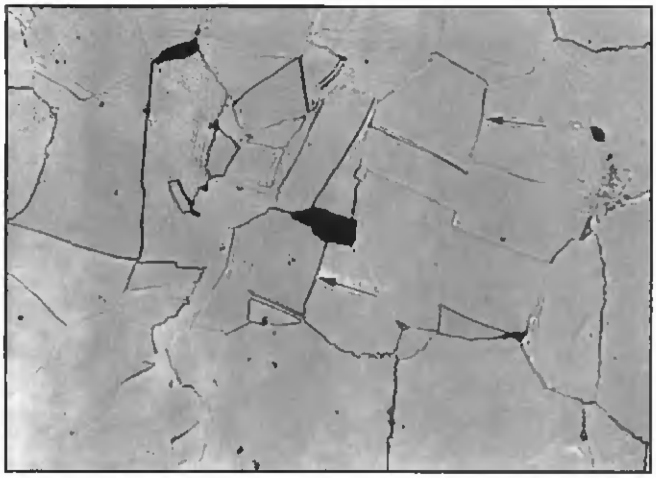

Fig. 9 — Microstructure of D2 after 800°C relaxation test (400X) showing clean grain boundaries again after migration by growth.

Fig. 10 — Microstructure of A1 after 850°C relaxation test (400X) showing grain boundaries free of precipitates.

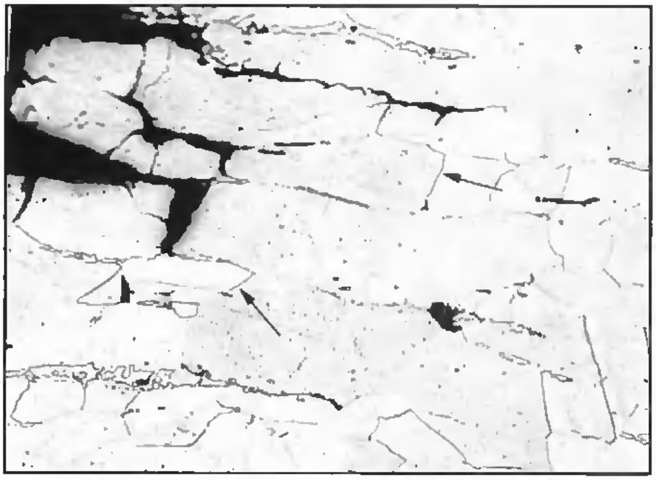

Fig. 11 — Microstructure of C2 after 850°C relaxation test (400X) showing austenitic grain boundaries free of precipitates

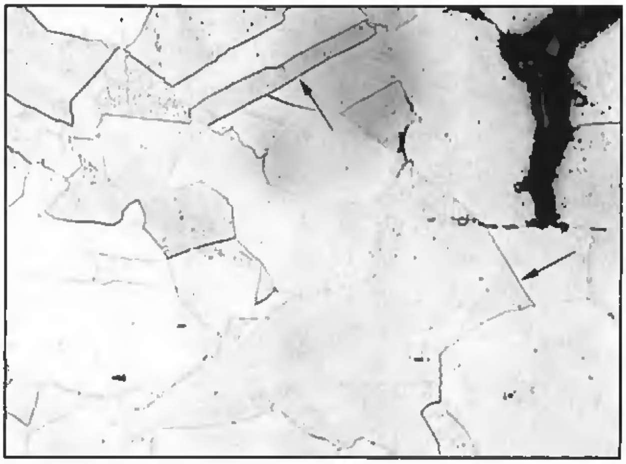

Fig. 12 — Microstructure of D1 after 800°C relaxation test (400X) showing austenitic grain boundaries free of precipitates.

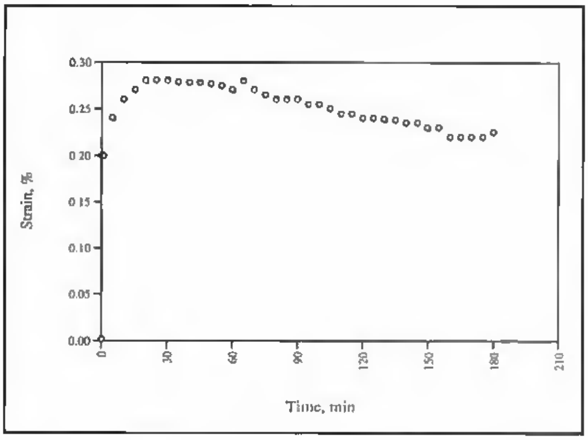

Fig. 13 — A strain vs. time curve from constant stress tests of C2 at 750°C (reproduced from representative strain vs. time strip chart recording) showing shrinkage with aging.

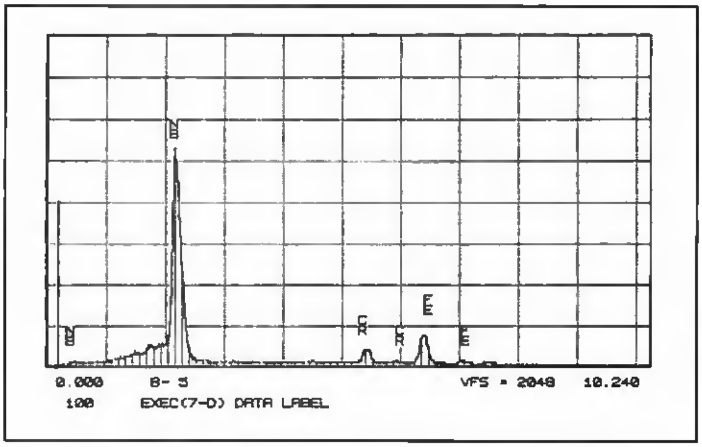

Fig. 14 — EDS analysis of an intragranular precipitate in C2 after 750°C relaxation test, showing strong presence of Nb.

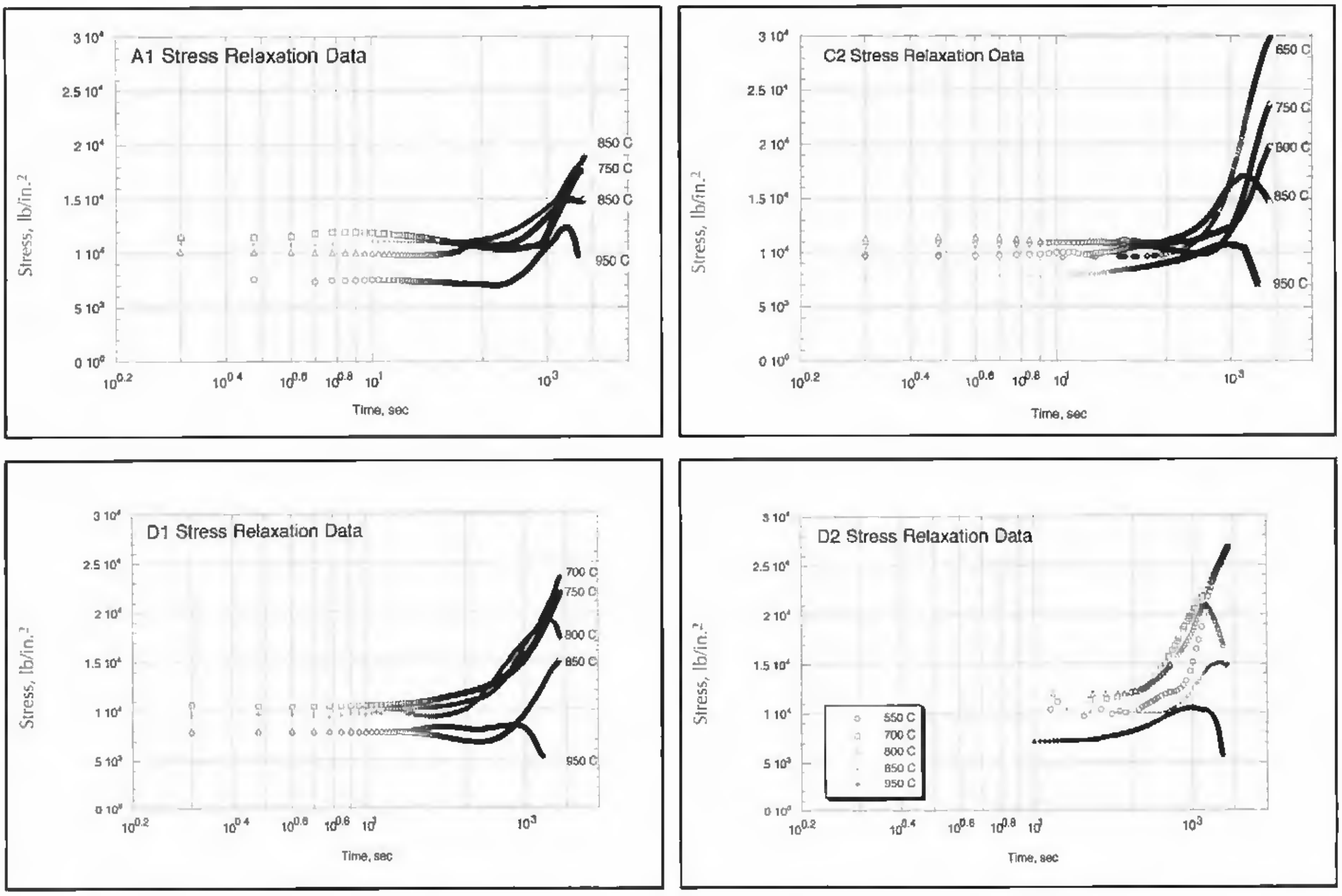

Fig. 15 — Stress relaxation curves plotted as stress vs. logarithmic time: A — Heat A1; B — heat C2; C — heat D1; D — heat D2.

where σ is the engineering stress at the notch, σ_0 is the initial stress level at the start of relaxation, k is the slope of the line (which can be considered as the relaxation modulus) and t is time. This equation shows stress relaxation seems to occur according to a logarithmic relationship observed in other studies (Refs. 15, 16).

Precipitation of Nb carbides is believed to start at the point where the relaxation curve loses linearity by bending upward. From the curves shown in Fig. 15, precipitation start times are obtained and plotted as precipitation-time-temperature (PTT) curves — Fig. 16. These PTT curves exhibit a C-shape, which is typical for precipitation kinetics (Ref. 16). Test material D2, which is the most susceptible to reheat cracking, shows the shortest nose time in its precipitation C-curve. It is known that the closer the Nb:C ratio is to 7.7, the stoichiometric composition of niobium carbide, the greater the potential for precipitation (Ref. 17). In the present study, the Nb:C ratio for A1, C2, D1 and D2 (Table 1) are 18.2, 11.8, 16 and 10.9, respectively, with D2 being the closest to 7.7. When C2 and D2 are compared, it is noticeable they have almost the same Nb:C ratio, yet C2 is more sluggish in precipitation kinetics than D2. This result shows other chemical effects also influence precipitation kinetics. Since C2 contains 25 times more sulfur than D2, it seems reasonable to suggest that sulfur, which strongly segregates to interfaces, may have caused a slower precipitation reaction in C2. However, further investigation is needed to positively identify these chemical factors. Nitrogen content and ferrite potential may also affect the precipitation kinetics.

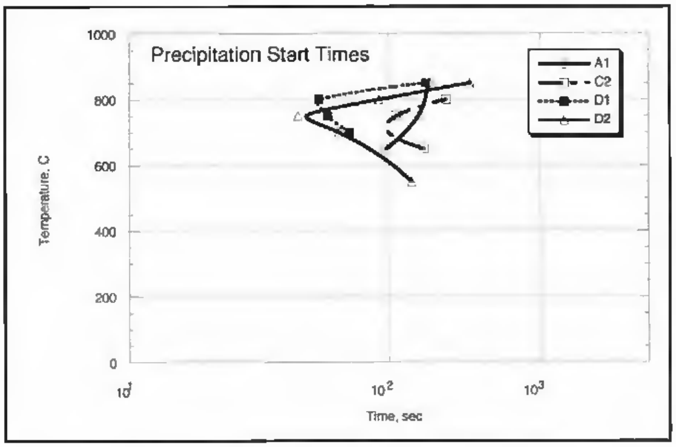

Fig. 16 — Precipitation start times plotted in the format of precipitation-time-temperature (PTT) diagram.

From the preceding, it is reasonable to assume that reheat cracking during postweld heat treatment is driven by the precipitation behavior of the alloy. Approaches to circumventing the reheat cracking problem should be considered in light of factors affecting such precipitation. For example, compositional adjustments and control of thermal-mechanical treatment may allow reheat cracking to be circumvented.

Conclusions

1) A Gleeble-based test was employed

to evaluate reheat cracking during PWHT of Type 347 stainless steel, with considerations taken for microstructure, change of strength with temperature, and stress levels to simulate reheat cracking conditions. This test has been used by others as well (Refs. 7, 10).

2) The increase of force (stress) vs. relaxation time observed for all test compositions was attributed to volumetric shrinkage upon precipitation of Nb-rich particles; this increase is believed to contribute to reheat cracking in the presence of a precipitate-hardened matrix under rigid restraint.

3) A verification test under constant-load conditions produced a small but definite decrease in strain vs. time, supporting the contention that a volume (or density) change occurs during a complicated precipitation and stress-relaxation process.

Acknowledgments

The authors would like to thank the WRC High Alloys Committee and Stainless Steel Welding Subcommittee for financial and technical support of the work reported here. Discussions with Dr. H. Ferguson and Dr. W. Chen, DSI, Inc., and technical assistance from D. Van Steele, manager of the mechanical testing lab at RPI, are also gratefully acknowledged.

References

1. Messler, R. W., Jr., and Li, L. 1997. Weld heat-affected zone liquation cracking in Type 347 stainless steel. *Science and Technology of Welding and Joining* 2(2): 43–52.

2. Easterling, K. 1992. *Introduction to the Physical Metallurgy of Welding*, Second ed. Boston, Mass., Butterworth-Heinemann.

3. Cordea, J. N. 1975. Niobium- and vanadium-containing steels for pressure vessel service. Bulletin 203. New York, N.Y., Welding Research Council, pp. 33–34.

4. Thomas, R. D., Jr. 1984. HAZ cracking in thick sections of austenitic stainless steels — part II. *Welding Journal* 63(12): 355-s to 368-s.

5. Younger, R. N., and Baker, R. G. 1961. Heat-affected zone cracking in welded austenitic steels during heat treatment, Report B5/11/61, British Welding Research Association, pp. 579–587.

6. Christoffel, R. J. 1962. Cracking in Type 347 heat-affected zone during stress relaxation. *Welding Journal* 41(6): 251-s to 256-s.

7. Franklin, J. E., and Savage, W. F. 1974. Stress relaxation and strain-age cracking in Rene 41 weldments. *Welding Journal* 53(9): 380-s to 387-s.

8. Widgery, D. J., Howard, R. D., McKeown, D., and Gooch, T. G. 1972. The development of criteria for the assessment of welding characteristics of high temperature materials: progress in general applicability evaluation. TWI Final Report no. 3270/13/72, pp. 1–33.

9. Ishii, J., Kaihara, S., and Kume, R. 1995. Reheat cracking sensitivity of the welded joint of austenitic stainless steel, IIW Doc. IX-1787-94.

10. Lin, W., and Lippold, J. C. 1995. Evaluation of postweld heat treatment cracking in nickel-based alloys and stainless steels. Paper presented at 76th AWS Annual Meeting, Cleveland, Ohio.

11. Karjalainen, L. P. 1995. Stress relaxation methods for investigation of softening kinetics in hot deformed steels. *Materials Science and Technology* 11(6): 557–565.

12. *ASM Handbook*, Vol. 20, Materials Selection and Design. 1997. Materials Park, Ohio, ASM International, pp. 510–511.

13. Yue, M. S., and Jonas, J. J. 1991. Hot ductility of steels and its relationship to the problem of transverse cracking during continuous casting. *International Materials Reviews* 36(5): 187–217.

14. Dieter, G. E. 1976. *Mechanical Metallurgy*, New York, N.Y., McGraw Hill, pp. 473–476.

15. Gibbs, G. B. 1966. Creep and stress relaxation studies with polycrystalline magnesium. *Phil. Mag.* 13: 317–329.

16. Liu, W. J., and Jonas, J. J. 1988. A stress relaxation method for following carbonitride precipitation in austenite at hot working temperatures. *Met. Trans. A*: 19A(6): 1403–1413.

17. Keown, S. R., and Pickering, F. B. 1981. Niobium in stainless steels. *Niobium, Proceedings of the International Symposium*, San Francisco, Calif., pp. 1113–1141.